university of groningen / faculty of science and engineering

Evaluation of continuous bed motion and the reconstruction parameters for the Biograph Quadra whole body PET/CT scanner using EARL accreditation and associated image quality

Author:
Sandro EL WADI
(s4887611)

Supervisor:
dr. Sasha IVASHCHENKO
Second examiner :
prof. Antoon WILLEMSEN

Bachelor's Thesis
To fulfill the requirements for the degree of
Bachelor of Biomedical Engineering
at the University of Groningen

August 1, 2024

Contents

Page

Abstract **3**

Acknowledgements **4**

1 Introduction **5**
1.1 PET/CT imaging 5
1.2 EANM 6
1.2.1 EARL Accreditation 6
1.3 Aim 7
1.4 Research Questions 7
1.5 Thesis Outline 8

2 Materials and Methods **9**
2.1 Quadra PET/CT system 9
2.2 NEMA phantom 10
2.3 F-18 radiotracer 11
2.4 Reconstruction parameters and other variables 11
2.5 Evaluation of data 12

3 Results and Discussion **14**
3.1 Raw data and calculations 14
3.2 RCmean vs EARL 2 limits 14
3.3 RCmax vs EARL 2 limits 17
3.4 Comparison of Gaussian filters vs EARL 2 limits 19

4 Conclusion **22**

Bibliography **23**

Appendices **26**
A Sigma to FWHM conversions 26

Abstract

The technological development of PET/CT scanners over the past 20 years has been staggering. Starting from a traditional PET/CT scanner, improvements on sensitivity, axial field of view, dose required, and speed of scan acquisition were all made. This allowed for the development of whole body PET/CT scanners such as the ”Biograph Vision Quadra” that is presented with 2 modes of functionality, step-and-shoot and continuous bed motion. The research presented here aims to study the compliance of the CBM mode at varying speeds compared to its static counterpart using the EARL 2 parameters provided by EANM as a reference. Proper reconstruction parameters were also monitored and tested. The software 3D slicer was used for the image analysis. This report demonstrates the EARL compliance of the CBM modes whilst also finding the ideal reconstruction parameters required, in this case a 4 mm Gaussian filter. Moreover, the speed of image acquisition was also studied using a statistical test. Further research using more prominent samples or improved software will result in a better understanding of the proper parameters to be used allowing for multi center studies to take place with this new scanner.

Acknowledgments

I would like to express my sincerest gratitude to **Prof. Dr. Sasha Ivashchenko** for giving me the chance to conduct this research under your supervision. Your continuous support has helped me develop my research, academic writing, and presentation skills throughout this project while teaching me a very interesting topic in Medical Imaging.

You also taught me how to use the instrumentation and the theoretical concepts needed to conduct this research wonderfully.
I am glad I chose to do my research with you, and I wish you the utmost success in your future projects.

Finally, I would like to thank my family and friends for the constant emotional and mental support they have provided throughout the project. I couldn't have done it without you guys!

1 Introduction

The start of this century marked the first commercial installations of hybrid positron emission tomography and computed tomography (PET/CT) with a field of view of 25.6 cm. [1] This relatively new technology has since then become the standard of care for patients in the field of oncology. This technological adoption is accompanied by continuous enhancement of performance due to all the innovations that have been discovered and implemented. In more recent years, PET technology experienced development as it was confirmed that increasing the sensitivity using an extended axial field of view (aFOV) would be possible. Volume sensitivity, is defined as the number of detected true events per unit time for each unit of activity present within a source [2]. Therefore its increase would be only beneficial for oncologists and their patients. This newfound knowledge pushed big healthcare corporations and research universities to find ways to start developing PET/CT technologies with the goal of increasing the aFOV as well as developing other parameters even further. In 2018 Siemens Healthlineers and UC Davis (Knoxville, TN, USA) introduced the "mini Explorer" with an aFOV of 45.7 cm. This was followed shortly after by the University of Pennsylvania and Philips Healthcare presenting their own PET/CT scanner called the "PennPET Explorer" allowing for aFOV's of 64 to 143 cm [3]. Finally in 2020 the "Biograph Vision Quadra" PET/CT system ("Quadra") by Siemens Healthineers (Knoxville, TN, USA) with an aFOV of 106 cm offering anatomical coverage roughly from head to thighs was introduced marking the peak of advancement in this sector as it stands [4]. Now that we've introduced the various PET technologies including the one used in the study, the next section will explain PET/CT as a whole.

1.1 PET/CT imaging

Before delving into PET/CT imaging a short description on both technologies is displayed. A radiotracer or radio-pharmaceutical is a small dose of radioactive substance that is injected into the human body or any test phantom for the sake of PET imaging. This substance will in turn release positrons (positively charged particles). Positron emission is the process in which a positron and an electron collide and destroy each other within the human body. This annihilation of the particles releases gamma rays that are picked up by the PET scanner. When producing the images, the scanner relies on the distribution of these gamma rays as they show metabolic activity on a cellular level which is beneficial for locating regions of aberrant cell development, such as cancer for example [5].
Contrarily, computed tomography (CT) uses X-ray technology providing fine grained cross-sectional images including the body's interior components. A computer then reconstructs these images allowing for improved accuracy of the body's anatomy. CT scanner application is intended to spot structural anomalies such as tumors, fractures or vascular problems. [6]
As mentioned above the hybridisation of these technologies allows to push the boundaries of medical imaging even further. This hybrid system allows to facilitate and localize diseases since 2 types of images are performed through one scanner system through a method of fusion. These conventional PET/CT systems with their short axial field of view (SAFOV) have a typical sensitivity level of 6-20 cps/kBq [7].The majority of the body would be outside of the FOV thus allowing for a small percentage to be picked up as a signal. However, these traditional scanners were met with more advancements such as the increase of sensitivity and axial field of view as can be seen with the "Biograph Vision Quadra" which would have a sensitivity of 83 cps/kBq. An increase of sensitivity by 5x is thus displayed [8].
These systems also have 2 functional modes. Firstly step-and-shoot which essentially, if we were working with a whole body scan would have to take multiple acquisitions to perform. Whilst it would

have a uniform sensitivity profile due to the scans being performed while stationary, this would also prolong the scan duration thus reducing the patients comfort and slowing down the entire process. Then we have continuous bed motion, this function allows for the scan to be acquired all in one go which varies the sensitivity profile throughout the scan length. This variation can always be adjusted when reconstructing the image. This ensures more uniform results with the possibility of a very slight lower image quality compared to its counterpart. However it is definitely more smooth and comfortable for the patient and provides faster all round acquisitions. Since both modes clearly have advantages and disadvantages, their function should be based on the study being done. If the scans required are precise and short, step-and-shoot would be more advisable but if whole body scans are required CBM will be the better modality to be used. [9] This will further be confirmed throughout this study.

1.2 EANM

The European Association of Nuclear Medicine, was set up in 1985 and has been continually evolving [10]. This allows them to keep up with the pace of technological innovations in the realm of nuclear medicine. In 2006, they founded the EANM Research Gmbh (EARL) which imposes specific guidelines that should be respected. This allows for **harmonization of quantification** in the field. Furthermore, this allows for a contact point between researchers, clinicians and business leaders as all data will be relatively comparable. This in turn also pushes nuclear medicine into the agenda of EU research.
The following subsection will allow for a much deeper insight on these specifications and how they came about over the years.

1.2.1 EARL Accreditation

In 2010, EARL set up the ”EARL FDG PET/CT” accreditation and its quantification synchronisation program to allow for clear and uniform data whilst also preventing different patient diagnoses depending on the imaging center where the scan was performed [11]. A few benefits of seeking this accreditation were mentioned above. These also include enabling quality control and assurance thus allowing for repeatability and the ability for comparison when working with new equipment or when performing multi-center research projects. However, in 2018 due to all the improvements in the field notably with the addition of point spread function (PSF) and time of flight (TOF) modules, the accreditation was once again updated providing a second set of F-18 radio-tracer standards to be respected. These were discovered by Andres Kaalep et al. in their own study testing the PET/CT systems for performance harmonisation [12]. This second set of limits will be the standards monitored throughout this study as they are more refined and provide more accurate comparative data.
The accreditation is based on a quality control test using the NEMA IQ phantom and follows three distinct parameters which can all be calculated using the standardized uptake values provided by the images. All three have an upper and a lower limit in terms of recovery coefficients for each of the NEMA spheres.
First, RC-mean which is based on the mean concentration of radioactivity determined by tomographic imaging within the volumes of interest (VOI) divided by the true activity concentration. Based on the six sphere sizes, the RC values should be between 1.00 and 0.39 with more actual details provided in the figure below.
Following that, RC-max which is theoretically similar but in this case, the maximal activity concentration within the VOI will be displayed. Its values will be in the range of 1.38 to 0.52.

Lastly, RC-peak which is a parameter that is still under revision was not tested in this study but can hypothetically be obtained by placing 12 mm diameter segmentation on all the VOI's in order to obtain the highest uptake value. [13]
The limits will be displayed below in a table provided by EANM.

NEMA IEC phantom spheres		^{18}F standards 1 RCs		^{18}F standards 2 RCs		
Diameter (mm)	Volume (mL)	max	mean	max*	mean	peak**
37	26.52	0.95 – 1.16	0.76 – 0.89	1.05 – 1.29	0.85 – 1.00	0.90 – 1.10
28	11.49	0.91 – 1.13	0.72 – 0.85	1.01 – 1.26	0.82 – 0.97	0.90 – 1.10
22	5.57	0.83 – 1.09	0.63 – 0.78	1.01 – 1.32	0.80 – 0.99	0.90 – 1.10
17	2.57	0.73 – 1.01	0.57 – 0.73	1.00 – 1.38	0.76 – 0.97	0.75 – 0.99
13	1.15	0.59 – 0.85	0.44 – 0.60	0.85 – 1.22	0.63 – 0.86	0.45 – 0.70
10	0.52	0.34 – 0.57	0.27 – 0.43	0.52 – 0.88	0.39 – 0.61	0.27 – 0.41

Table 1: ***F-18 EARL standards for RC's.*** *These are the first and second standards published by EANM for the NEMA IEC phantom spheres.*[13]

1.3 Aim

In order to be able to use the "Biograph Vision Quadra" in its continuous bed motion mode more for multi-centre studies or for comparisons with local and conventional PET/CT scanners, compliance with the EARL guidelines provided by the European Association of Nuclear Medicine (EANM) is required as these parameters have not been yet evaluated for this type of scanner functionality

Therefore, in the current study, using a NEMA IEC whole body phantom and the F-18 radiotracer along with the "Quadra" scanner, the effect of continuous bed motion (CBM) on quantification accuracy for PET/CT will be tested. For that, comparisons with the current EARL 2 accredited setting for static scan will be made using the EARL 2 limits as a reference.

Furthermore, ideal reconstruction parameters will be monitored and modified to ensure that all points of data will fit the necessary limits. The 3 modes of speed will also be compared.

1.4 Research Questions

To summarize, this report focuses on the following problems:

Q1. What is the effect of continuous bed motion at different speeds on the quantification accuracy for the Quadra scanner? Use the static scan and EARL 2 as references

Q2. Which reconstruction parameters and settings should be modified to allow for full compliance of the EARL accreditation? Are the settings also speed specific?

1.5 Thesis Outline

This paper will first present the materials and methods used to collect data which are described in detail. Followed by the results that will also be discussed before the paper is concluded and the research questions answered.

2 Materials and Methods

2.1 Quadra PET/CT system

All measurements and images used in this study were gathered using the ”Biograph Vision Quadra” PET/CT system created by Siemens Healthlineers [14]. The scanner is installed in the University Medical Center of Groningen (UMCG). It combines four conventional detectors into one system thus allowing for the 106 cm axial field of view.

The scanners technical specifications can be split up into two categories. First and foremost, the gantry, which has a diameter of 78 cm and a length of 235 cm with a capacity of 227 kg. This allows for the accommodation of most patients globally.

Secondly, the PET/CT specifications, 3.2×3.2×20 mm lutetium oxyorthosilicate (LSO) crystals coupled to silicon photomultipliers (SiPMs) which covers 100 % of the scintillator area. This then offers a time-of-fight (TOF) resolution of 228 ps which is a gain of 5.9x [15]. All these improvements regarding the PET/CT parameters, lead to the amplification of scanner sensitivity which in turn results in lower doses and faster scans. This scanner also comes in 2 modes, step and shoot as well as continuous bed motion each having its own precise functions as mentioned previously.

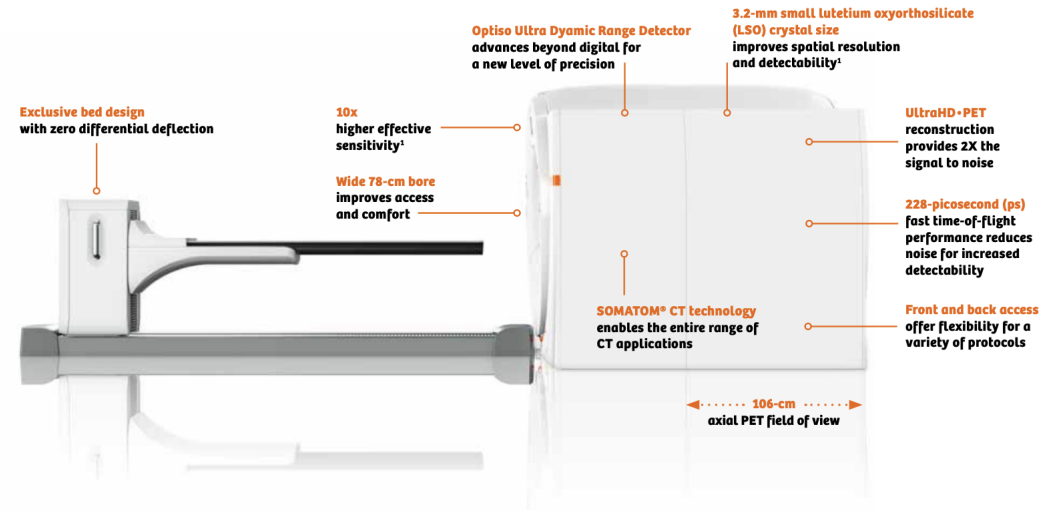

Figure 1: ***Biograph Vision Quadra PET/CT with a few of its technological improvements.*** [14]

From a more general outlook, this system and all its innovation will allow for the expansion of research dimensions due to its increased field of view, reshaping clinical outcomes thanks to its improved image quality relative to its scan time and dose and somehow still fits realistically in most hospitals since its size is similar to its traditional counterpart as can be seen in figure 3 below.

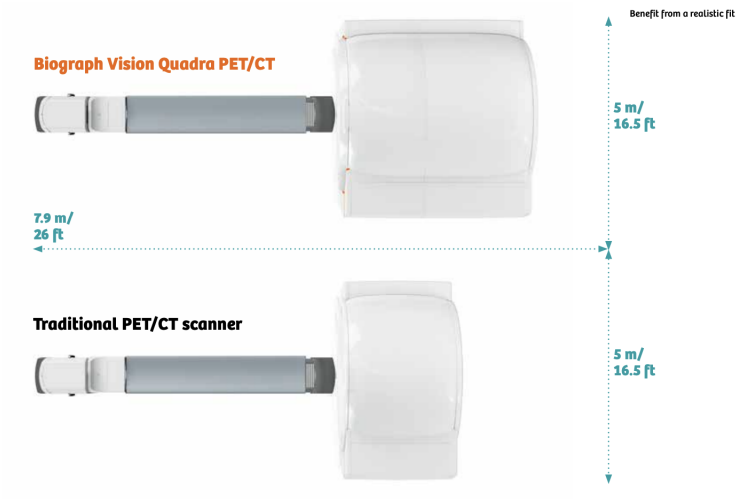

Figure 2: ***Scale of Quadra PET/CT vs. Traditional PET/CT scanner*** [14]

2.2 NEMA phantom

A NEMA IEC PET body phantom was used to gather all the data for this study. It is composed of six different size spheres that can be filled. The sizes are as follows; 37 mm, 28 mm, 22 mm, 17 mm, 13 mm and 10 mm [16]. It was filled up with distilled water and a radio tracer allowing to evaluate the reconstructed image quality of any PET based scanner. Since we are working with the EARL 2 guidelines, the activity concentrations within the spheres should be between 18 to 22 kBq/ml with a background activity concentration ranging between 1.8 to 2.2 kBq/ml [17] [13]. This is due to the 10:1 sphere to background ratio. This in turn means that in the background the phantom was filled up to 10 L with 25 Mbq [18]. Assessment of these activity concentrations will be further displayed in the results section.
For this study specifically, the patient aka the phantom had a weight of 62 kg. This is a crucial parameter as it will be useful when calculating the recovery coefficients in following sections.

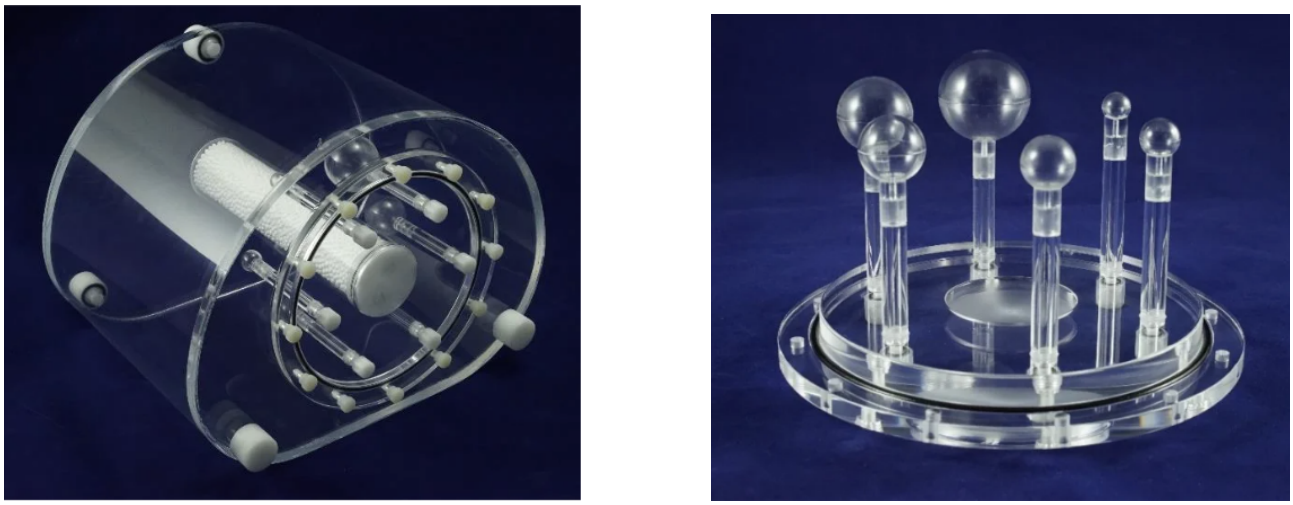

Figure 3: ***NEMA phantom and its spheres*** [16]

2.3 F-18 radiotracer

Fluodeoxyglucose, F-18 is a radiotracer that acts similar to glucose. This isotope is mostly used for diagnostic purposes or in conjugation with PET situations as it allows to localize tissues that have any alterations in glucose metabolism. It is crucial to spot these changes within the metabolism as they have implications for malignancies, epilepsy, myocardial ischemia, inflammatory conditions, and Alzheimer disease [19].

F-18 can be used in many different medical fields but focusing solely on oncology, this radiotracer is FDA approved for evaluating, monitoring and staging treatment for various types of cancers.

For our study the dose injected in the one liter stock solution that is then inserted in the spheres of the phantom was 25 MBq (MBecquerel), or alternatively 25 kBq/ml. Just like the weight mentioned earlier, this will also be a parameter to take into account for any further calculations.

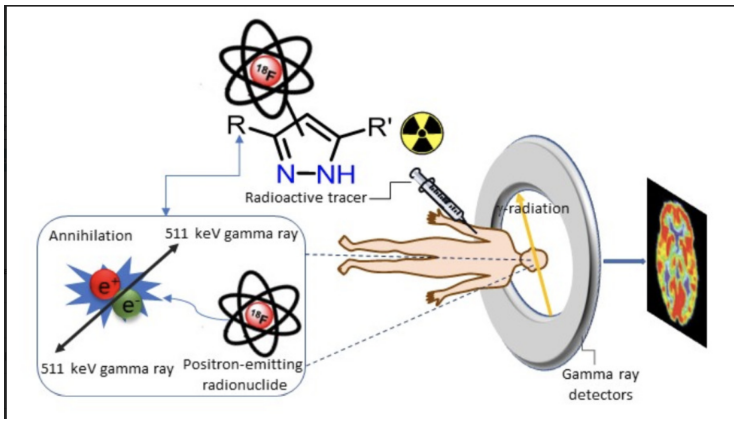

Figure 4: ***Image depicting the role of the F-18 radiotracer in PET scans*** [20]

2.4 Reconstruction parameters and other variables

There are certain crucial parameters and variables to take into account when working with the Quadra PET/CT which will be discussed in a bit more detail in this section.

First and foremost, the methods of reconstruction for the images were all whole body (WB) and continuous bed motion (CBM) with the point spread function (PSF) modality which is used to describe what a single point in the object looks like in the image. Since the acquired image is always a blurred representation of the actual object, by using PSF the process of image formation will be rendered mathematical as it would just be the object convoluted with the imaging setup's PSF which gives the acquired image [21].

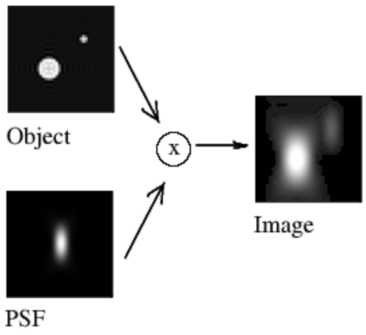

Figure 5: ***Image displaying the functionality of point spread function***[21]

PSF is also linked with the time of flight response (TOF) which as mentioned previously is beneficial for sensitivity increase. The combination of both parameters increases the image quality as a whole [22]. All the images were reconstructed using 4 iterations and 5 subsets, 708 slices, with a matrix size of 220 x 220 which results in isotropic voxel size (pixel size) of 3.3 x 3.3 mm^3. Within the 17 images, 9 had a maximum ring difference (MRD) of 322 whilst the other 8 were at an MRD of 85. This is simply put, the maximal axial acceptance angle [23]. It is also important to note that all these images were corrected by applying decay and scatter correction as a lack of these additional parameters would cause issues in terms of noise when looking at scans that were taken over an hour past the original injection time.
Furthermore, using these reconstruction methods and variables the scans were split to facilitate comparisons. The scans were based on 3 continuous bed motion speeds. A total of 8 scans per Gaussian filter. They would be split in sample sizes of 2, 3 and 3 with speeds, 6.4 mm/s, 3.2 mm/s and 1.6 mm/s respectively.
All the most important informative data on the parameters for this study can be found in the table below.

Acquisition speed	Number of scans	Reconstruction methods	Pixel spacing	Matrix size	Kernel	Nbr of slices	Series start time	Radiopharmaceutical start time	CBM or Static	Weight (kg)	Activity (Mbq)
EARL STATIC	1	WB PSF + TOF 4i 5s RD85	3.3, 3.3	220x220	XYZ Gauss 5.00	708	17:36	17:34	STATIC	10	20
6.4 mm/s	2	WB PSF + TOF 4i 5s RD322/85	3.3, 3.3	220x220	XYZ Gauss 3, 4, 5	708	11:32, 11:40	11:00	CBM	62	25
3.2 mm/s	3	WB PSF + TOF 4i 5s RD322/85	3.3, 3.3	220x220	XYZ Gauss 3, 4, 5	708	11:43, 11:49, 11:55	11:00	CBM	62	25
1.6 mm/s	3	WB PSF + TOF 4i 5s RD322/85	3.3, 3.3	220x220	XYZ Gauss 3, 4, 5	708	12:00, 12:12, 12:23	11:00	CBM	62	25

Table 2: ***All variables and reconstruction parameters for the scans***

2.5 Evaluation of data

Once all the data was obtained as a DICOM file, provided by the Quadra PET/CT scanner, the use of 3D slicer took place. 3D slicer, is a desktop software that's main focus is solving advanced imaging

computation challenges that have clinical and biomedical applications. It allows the deployment of custom solutions for research and is a very powerful tool for image analysis [24].
Using the DICOM header within the software allowed us to obtain all the necessary parameters that were mentioned above. Then by using specific tools within the program that will be briefly explained below, determining the SUV mean and max values for all 17 scans was possible followed by their combination into speed groups as mentioned above.
We used the CT modality to place the segmentations on all 6 regions of interest (ROI) using the segment editor tool. To avoid any additional noise the segmentations were placed with smaller sizes relative to their spheres. As we already know, the sphere sizes for the NEMA phantom are 37 mm, 28 mm, 22 mm, 17 mm, 13 mm and 10 mm. The segmentations had sizes of 35 mm, 26 mm, 20 mm, 15 mm, 12 mm and 9 mm respectively. They would then be saved within the program to be used for all the other scans.
An example of the segmentations placed on one of the PET scans will be displayed below.

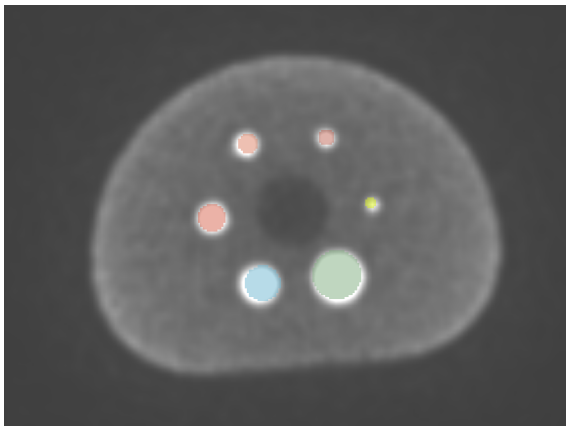

Figure 6: ***Image displaying the segmentations placed on the 6 VOI's***

The filtering tool was also used as it allows to set up a personal Gaussian filter by allowing to plug in the sigma value that is desired, matching with the full width half maximum value. In this study's case, since we had 5 mm and 3 mm FWHM values, we managed to determine the sigma value for the 4 mm FWHM which would be 1.39 [A]. This value would then be used in order to obtain an additional 8 scans with a convolution kernel of 4 mm.
Finally, using the quantification tool the values for SUV-mean and SUV-max based on the different sphere sizes were obtained. This is important as we would be using the SUV values as a way to determine the recovery coefficients.
Now that the image analysis using the program 3D slicer is complete, we ended up with a bunch of raw data to be processed further. This will be discussed thoroughly in the following section.

3 Results and Discussion

3.1 Raw data and calculations

Spheres	SUVmean	StDEV	Weight (g)	Activity (mCi)	Act conc. spheres (mCi/cc)	Noise mci/cc	Acc conc. spheres(Bq/cc)	Noise (bq/cc)	Theoretical activity conc. (Bq/cc)	Rcmean
37 mm	54.6707	11.9115	62000	0.67567568	0.0005958	0.00012981	22045	4803	25000	0.88
28 mm	51.7158	14.4758	62000	0.67567568	0.0005636	0.00015776	20853	5837	25000	0.83
22 mm	51.419	13.4166	62000	0.67567568	0.00056036	0.00014621	20733	5410	25000	0.83
17 mm	51.8381	11.8442	62000	0.67567568	0.00056493	0.00012908	20902	4776	25000	0.84
13 mm	46.8289	13.5485	62000	0.67567568	0.00051034	0.00014765	18883	5463	25000	0.76
10 mm	34.0825	14.829	62000	0.67567568	0.00037143	0.00016161	13743	5979	25000	0.55

Spheres	SUVmax	StDEV	Weight (g)	Activity (mCi)	Act conc. spheres (mCi/cc)	Noise mci/cc	Acc conc. spheres(Bq/cc)	Noise (bq/cc)	Theoretical activity conc. (Bq/cc)	Rcmax
37 mm	68.6149	11.9115	62000	0.67567568	0.00074776	0.00012981	27667	4803	25000	1.11
28 mm	68.5698	14.4758	62000	0.67567568	0.00074727	0.00015776	27649	5837	25000	1.11
22 mm	68.4162	13.4166	62000	0.67567568	0.0007456	0.00014621	27587	5410	25000	1.10
17 mm	68.4368	11.8442	62000	0.67567568	0.00074582	0.00012908	27595	4776	25000	1.10
13 mm	68.8249	13.5485	62000	0.67567568	0.00075005	0.00014765	27752	5463	25000	1.11
10 mm	59.7869	14.829	62000	0.67567568	0.00065156	0.00016161	24108	5979	25000	0.96

Figure 7: ***Example of RC-mean and RC-max calculation.*** *The final values will then be used for comparison with the EARL 2 limits*

The figure above provides an example of the calculations that took place in order to obtain the recovery coefficients. We can see the weight at 62000 g as mentioned previously. It is also known as well that the activity is 25 MBq as provided by the DICOM header. This is then converted to millicurie (mci) by simply dividing 25 by 37 which gives 0.67 roughly.
Now that all the necessary values have been obtained, we determined the activity concentration (mci/cc) [25].

$$Activityconc.(mci/cc) = SUV * (Actvity(mci)/Weight(g)) \tag{1}$$

This value would then be converted to Bq/cc by multiplying values with $37 * 10^6$. Finally, the RC mean or RC max value could mathematically be determined [26].

$$RC = Activityconc.spheres(Bq/cc)/TheoreticalActivityconc.(Bq/cc) \tag{2}$$

The theoretical activity concentration (Bq/cc) in this study would be thus be 25000 Bq/cc.
We then, used the same template for all 25 scans and placed them back into their speed subsections in order to obtain understandable graphs that would not be overcrowded.

3.2 RCmean vs EARL 2 limits

Throughout the experimental process, we tried optimizing the images by using different sizes of filters as they have the tendency to remove unwanted noise at different levels. This section will discuss the recovery coefficients at the mean standardized uptake values.
By looking at the different figures below, we can already spot that the scans that were reconstructed using the 3 and 4 mm Gaussian filters fit within the EARL 2 criteria at every single sphere size. This showed promise for the aforementioned filters. However, RC max would also need to be tested for full confirmation.

Unlike the other two kernels, the 5 mm filter did not fit within the limits. This is displayed in figure 10 along with its designated table 3c. As explained earlier, a scanner system must fit all 3 EARL provided standards in order to be properly accredited, with the RCmean being the most important of the 3. This allows us to stop considering the filter as a potential candidate making it an easier comparison between the smaller kernel sizes in the following sections.

Furthermore, when taking a closer look at these graphs we can see the presence of a red line indicating the reference static scan which is already accredited. Since this scan was acquired using a 5 mm Gaussian filter, its values being lower compared to the 3 and 4 mm filtered scans is logical as a bigger filter leads to more noise reduction. This is not the case, solely at sphere size 28 mm and could potentially be due to the motion which could in turn reduce the image quality slightly at certain sphere sizes. Other reasons that could prove the difference could be the weight and radiopharmaceutical used. As we know, the intial dynamic scans all had a weight of 62 kg and 25 MBq of injected dose. The static scan had a weight of 10 kg with 20 MBq of injected dose. Those clear differences can also apply when monitoring the discrepancy between the static and dynamic images. The red static scan does however perform better than its own 5 mm counterpart that didn't even fit the EARL limitations at its 3 speeds. So from an RCmean standpoint using a 3 or 4 mm filter would be correct resulting in EARL fitting values just like the static reference used.

Spheres	EARL 2 RCmean lower limit	EARL 2 RCmean upper limit	Speed 6.4	Speed 3.2	Speed 1.6	EARL STATIC
37	0.85	1	0.90	0.90	0.90	0.86
28	0.82	0.97	0.85	0.85	0.85	0.87
22	0.8	0.99	0.86	0.86	0.86	0.81
17	0.76	0.97	0.88	0.88	0.89	0.77
13	0.63	0.86	0.80	0.80	0.81	0.66
10	0.39	0.61	0.58	0.58	0.56	0.43

(a) Table RCmean Gauss 3

Spheres	EARL 2 RCmean lower limit	EARL 2 RCmean upper limit	Speed 6.4	Speed 3.2	Speed 1.6	EARL STATIC
37	0.85	1	0.89	0.88	0.88	0.86
28	0.82	0.97	0.84	0.83	0.83	0.87
22	0.8	0.99	0.83	0.83	0.83	0.81
17	0.76	0.97	0.84	0.84	0.85	0.77
13	0.63	0.86	0.74	0.75	0.75	0.66
10	0.39	0.61	0.53	0.53	0.51	0.43

(b) Table RCmean Gauss 4

Spheres	EARL 2 RCmean lower limit	EARL 2 RCmean upper limit	Speed 6.4	Speed 3.2	Speed 1.6	EARL STATIC
37	0.85	1	0.85	0.84	0.85	0.86
28	0.82	0.97	0.81	0.81	0.80	0.87
22	0.8	0.99	0.79	0.78	0.78	0.81
17	0.76	0.97	0.73	0.73	0.76	0.77
13	0.63	0.86	0.60	0.60	0.63	0.66
10	0.39	0.61	0.50	0.45	0.44	0.43

(c) Table RCmean Gauss 5

Table 3: RCmean values at all CBM speeds for all 3 filters vs Static values using EARL 2 limits as a reference

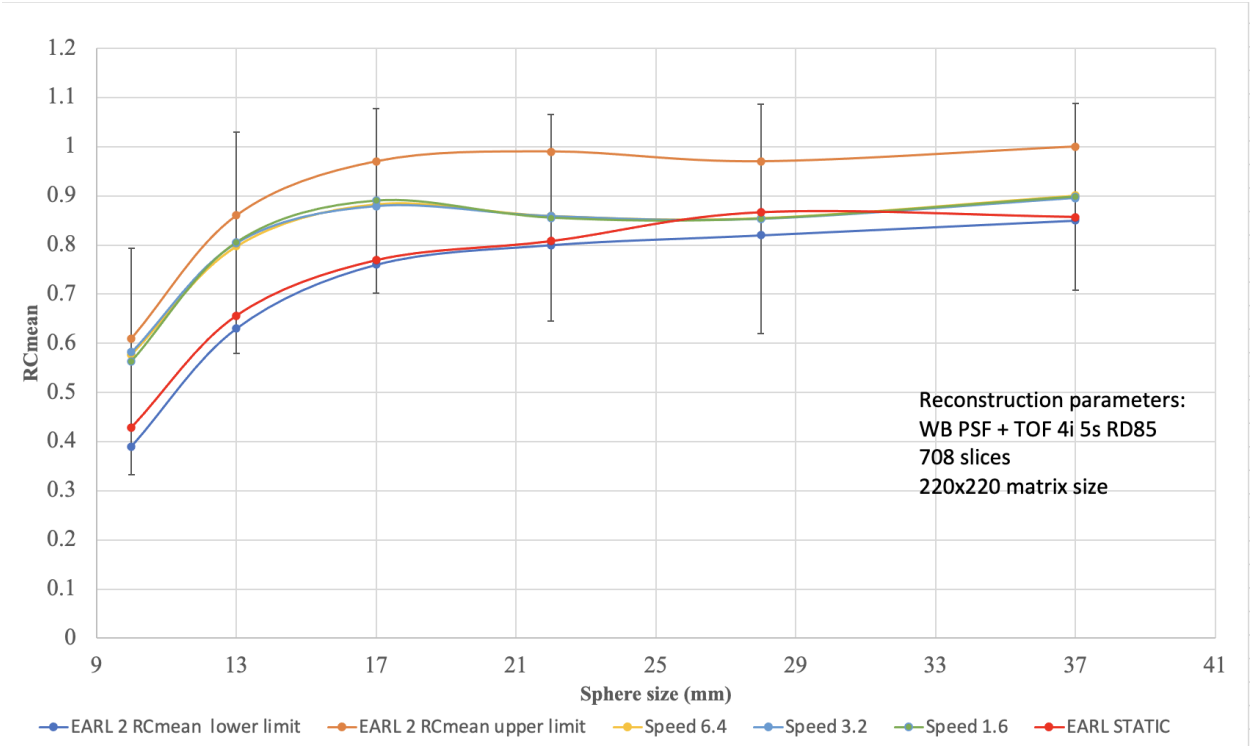

Figure 8: ***Graph RCmean Gauss 3mm vs Static scan using EARL 2 limits***

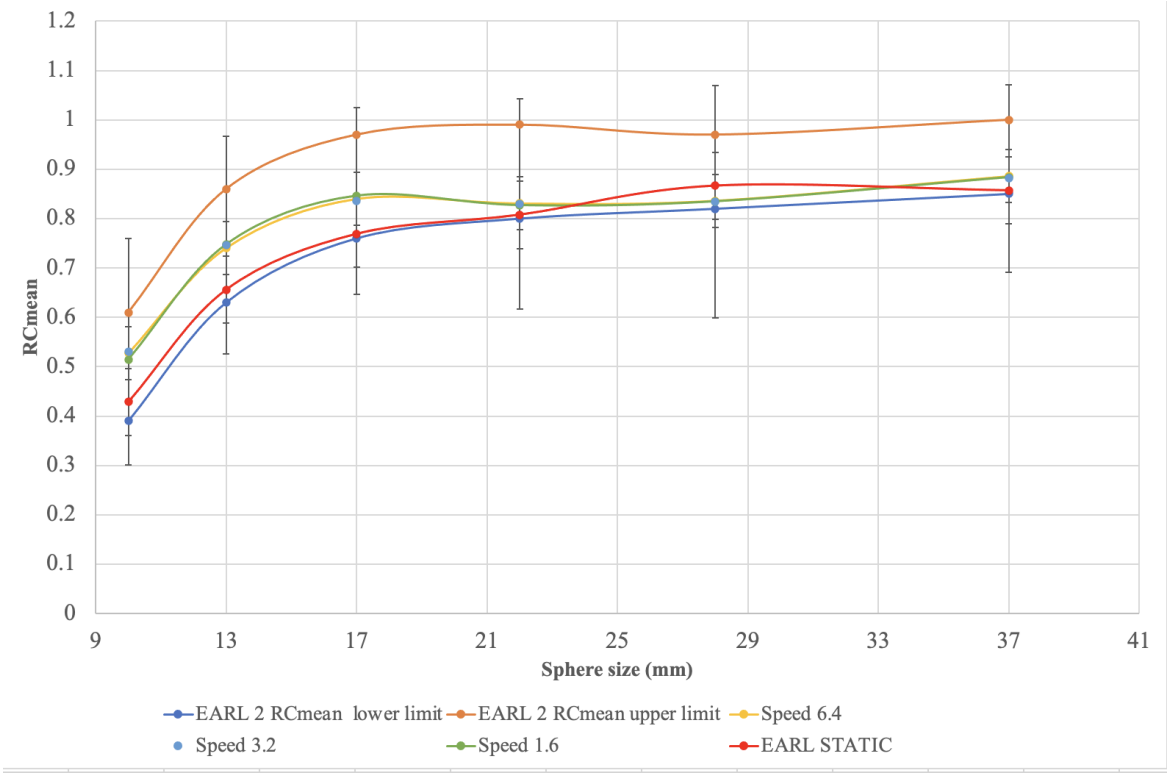

Figure 9: ***Graph RCmean Gauss 4mm vs Static scan using EARL 2 limits***

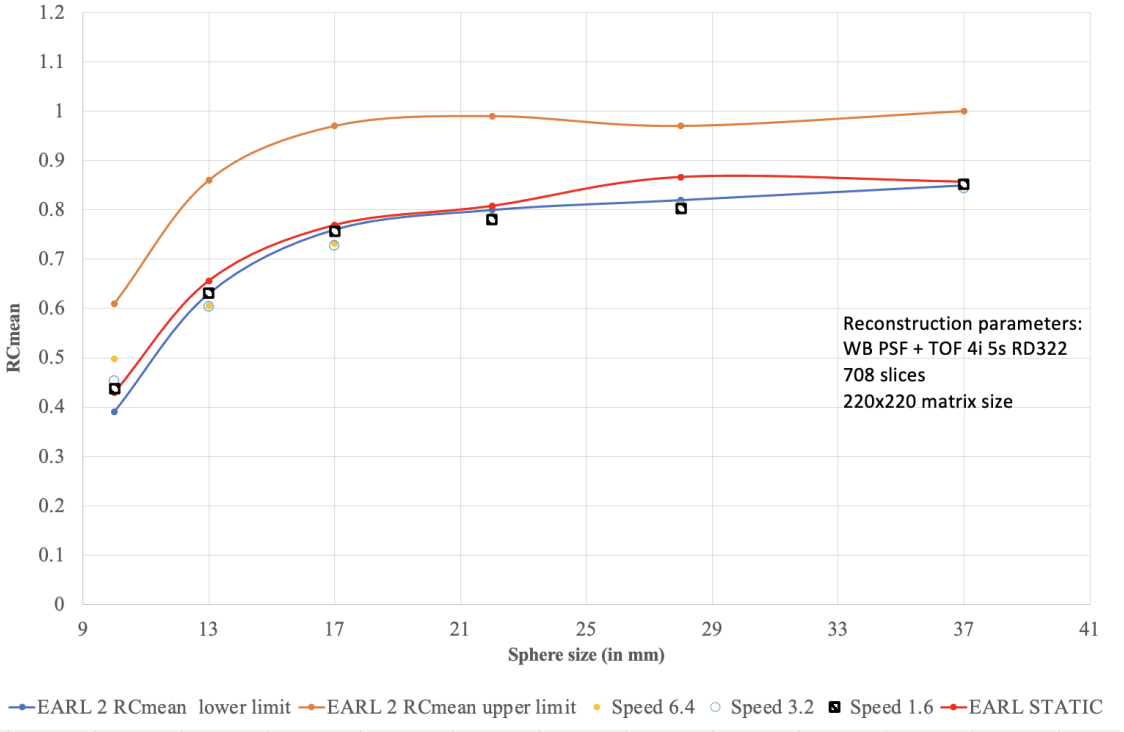

Figure 10: ***Graph RCmean Gauss 5mm vs Static scan using EARL 2 limits***

3.3 RCmax vs EARL 2 limits

Now that we've discussed the RC mean characteristics we can move to the RC max. As we know RC max takes the maximal value within a volume of interest thus giving the SUV maxes at all the different sphere sizes. Whilst we did determine and produce graphs for all 3 filter sizes, it was stated in the previous section that all the EARL parameters must be respected which was not the case for the RC mean values of the images using the 5 mm Gaussian filter. This is why this section will be discussing the 3 and 4 mm filtered images exclusively.

Table 4, along with figures 11 and 12 display all the information regarding the RC max values using the filters as well as the static scan. Firstly, we can see how the values for the static scan are still lower as explained earlier due to it being acquired with a 5 mm filter thus reducing noise more. We had also mentioned previously how the speed, weight and injected dose could affect the values present. These factors are thus valid for these 2 cases as both filters respect the EARL parameters whilst being at higher values relative to the static scan, up until the smallest sphere in the NEMA phantom (10 mm). However, when looking even deeper at both graphs we can see a more pronounced discrepancy between the 3 speeds and the EARL 2 upper bound limit in figure 11, representing the 3 mm filter. This is further confirmed by analysing and comparing the numbers in table 4. The 3mm filter at the 10 mm sphere would have an upper bound limit of 0.88 whilst the values would be 1.14, 1.09 and 1.08 for speed 6.4, 3.2 and 1.6 respectively whilst the 4 mm filter table has the same upper bound limit of 0.88 but with values 0.96, 0.93 and 0.92 for the same order of speed.

Spheres	EARL 2 RCmax lower limit	EARL 2 RCmax upper limit	Speed 6.4	Speed 3.2	Speed 1.6	EARL STATIC
37	1.05	1.29	1.19	1.16	1.15	1.12
28	1.01	1.26	1.23	1.16	1.14	1.10
22	1.01	1.32	1.20	1.16	1.14	1.07
17	1	1.38	1.20	1.16	1.16	1.06
13	0.85	1.22	1.22	1.20	1.21	0.99
10	0.52	0.88	1.14	1.09	1.08	0.67

(a) Table RCmax Gauss 3

Spheres	EARL 2 RCmax lower limit	EARL 2 RCmax upper limit	Speed 6.4	Speed 3.2	Speed 1.6	EARL STATIC
37	1.05	1.29	1.14	1.12	1.11	1.12
28	1.01	1.26	1.18	1.11	1.10	1.10
22	1.01	1.32	1.14	1.11	1.10	1.07
17	1	1.38	1.13	1.11	1.12	1.06
13	0.85	1.22	1.12	1.11	1.13	0.99
10	0.52	0.88	0.96	0.93	0.92	0.67

(b) Table RCmax Gauss 4

Table 4: ***RCmax values at all CBM speeds for all 3 filters vs Static values using EARL 2 limits as a reference***

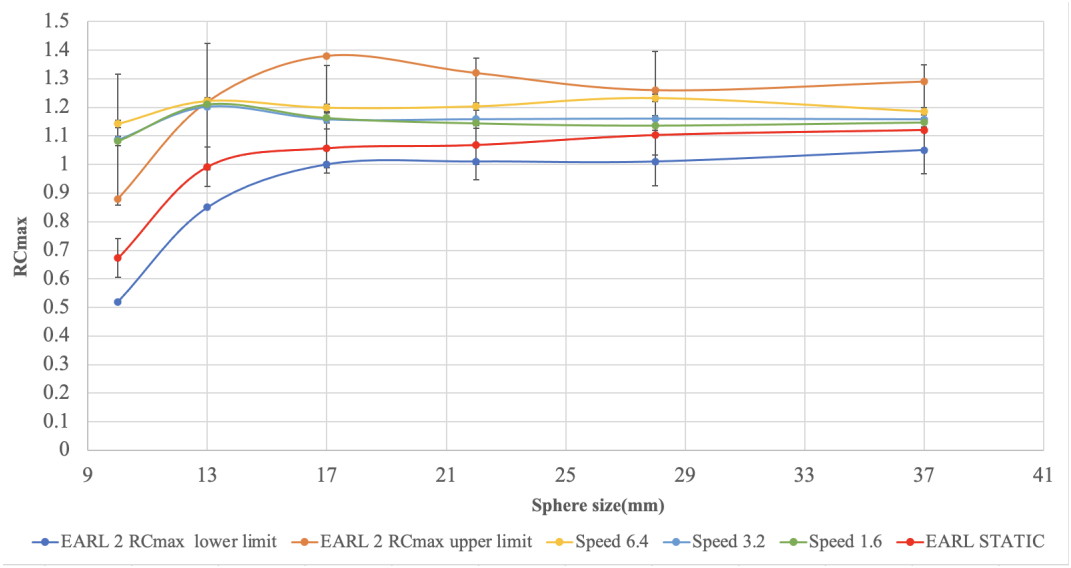

Figure 11: ***Graph RCmax Gauss 3mm vs Static scan using EARL 2 max limits***

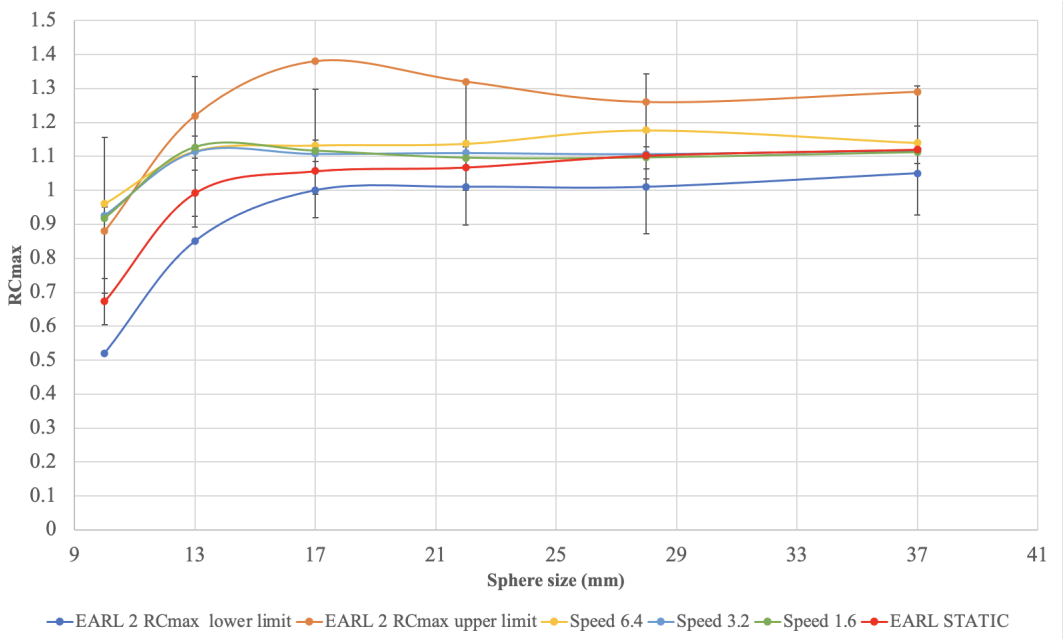

Figure 12: ***Graph RCmax Gauss 4mm vs Static scan using EARL 2 max limits***

There are a couple of potential reasons to explain the 10 mm sphere not fitting the limit in the RCmax graph. Noise, which can be an artifact that can disrupt the quality of an image is a very likely suitor [27]. Gibbs Artifact, or any type of edge artifacts are very likely to appear when working with smaller sphere sizes that have been reconstructed using the PSF module [28]. Due to the edges increased noise, the SUVmax will be increased thus causing the RC max not to properly fit within its limits. This would not happen for the mean recovery coefficients as they do not rely on the maximal values of SUV to determine the activity concentrations.

Time	Speed	AVG of all Spheres activity conc. (kBq/ml)	Background activity conc. (kBq/ml)	Ratio
11:00	filled	25	2.5	10 to 1
17:35	Static scan	20	2	10 to 1
11:35	6.4 mm/s	18	1.8	10 to 1
11:55	3.2 mm/s	18.4	1.84	10 to 1
12:12	1.6 mm/s	18.4	1.84	10 to 1

Table 5: ***Activity concentration at different speeds for 4 mm Gaussian filtered images***

Another possibility could be due to the time that the scans were taken. As we know based on the figure above which describes the activity concentration for the 4 mm filtered images, the F-18 radiopharmaceutical was added into the phantom at 11:00. Certain scans were taken over an hour later thus causing the radiotracer to get very close to its own half life of 109 minutes [19]. When assessing the activity concentration, an average of all spheres was performed for each of the speeds. The reason why the values are so close to the bottom of the range provided in section 2.2 is due to the 10 mm sphere. Whilst all other spheres had activities ranging around 20-22 kBq/ml, the 10 mm sphere would always have values around 12-14 kBq/ml thus diminishing the overall result. This would mean that at all time points the results would be valid with the EARL range except for the 10 mm sphere which deals with increased noise for the RCmax due to that.
After analysing all the information from the previous 2 sections, using the proper filter size at continuous bed motion will render similar quantification as its static counterpart. The variances could be due to the difference in filter size that can affect the amount of noise present as well as the speeds that could slightly hinder image quality. Further variations in weight and dose injected can also affect the recovery coefficients, but clearly not enough since all spheres fit the limit when applying proper reconstruction parameters.
The ideal image parametrization and will be fully confirmed below followed by a comparison of the continuous bed motion speeds.

3.4 Comparison of Gaussian filters vs EARL 2 limits

By looking at the two graphs and using all the information above regarding the RCmean and RCmax values in comparison to the EARL 2 limits, we can see that the yellow line representing the **Gaussian 4 mm filter** is the ideal fit when analysing images taken by the Quadra PET/CT scanner. **This would also be matched with a matrix size of 220 x 220, 708 slices, PSF + TOF, 4 iterations, 5 subsets, MRD 85 and by applying scatter and decay functionalities as well.** Although testing for RC peak is also usually necessary to complete the full EARL accreditation, the method of calculation proved to be faulty thus resulting in outcomes that did not fit the limits displayed in figure 1.

Spheres	EARL 2 RCmean lower limit	EARL 2 RCmean upper limit	Gauss 3	Gauss 4	Gauss 5
37	0.85	1	0.90	0.88	0.85
28	0.82	0.97	0.85	0.84	0.81
22	0.8	0.99	0.86	0.83	0.78
17	0.76	0.97	0.88	0.84	0.74
13	0.63	0.86	0.80	0.74	0.61
10	0.39	0.61	0.57	0.52	0.48

(a) RCmean filter comparison

	RCmax lower limit	RCmax upper limit	Gauss 3	Gauss 4	Gauss 5
37	1.05	1.29	1.16	1.12	1.06
28	1.01	1.26	1.18	1.13	1.07
22	1.01	1.32	1.17	1.11	1.04
17	1	1.38	1.17	1.12	1.04
13	0.85	1.22	1.21	1.12	0.95
10	0.52	0.88	1.10	0.94	0.70

(b) RCmax filter comparison

Table 6: ***Values comparing the 3 filter types with the EARL 2 limits.***Left: RCmean Right: RCmax

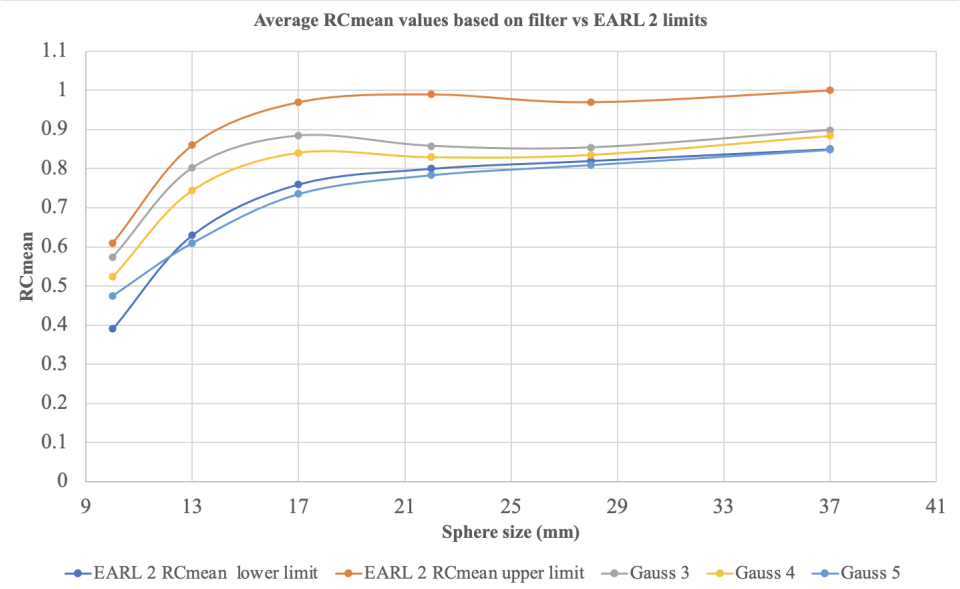

Figure 13: ***Graph RCmean filter comparison vs EARL 2 max limits***

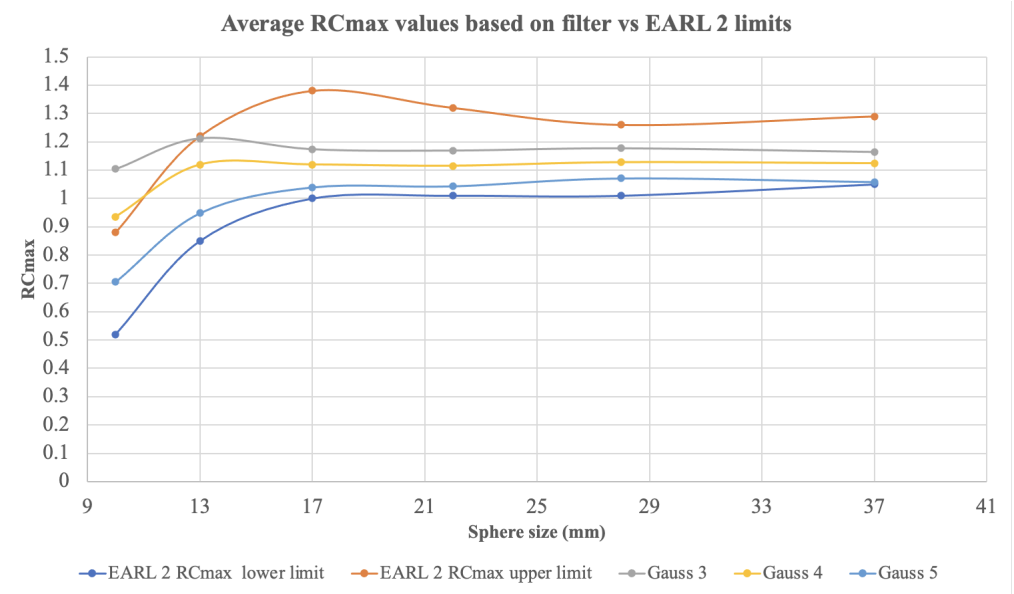

Figure 14: ***Graph RCmax filter comparison vs EARL 2 max limits***

Having obtained the ideal parameter for EARL accreditation, a statistical analysis on the speeds was performed for both RC mean and RC max of the 4 mm Gaussian filter. This would allow to compare between speeds whilst also checking if the reconstruction parameters are speed specific. For that by looking back at figure 7, we can see a section within the data named noise. Dividing it with the theoretical activity allows us to obtain the relevant standard deviations presented in table 7. These values along with the mean values are required to perform a t-test [29]

		Speed 6.4	Speed 3.2	Speed 1.6
Stdev for stats analysis		0.19	0.19	0.19
		0.24	0.24	0.23
		0.21	0.21	0.21
		0.19	0.19	0.19
		0.23	0.22	0.23
		0.25	0.23	0.23

Table 7: ***Standard deviation for both RC's with a 4 mm filter***

Using the RC mean values belonging to the 4 mm filter in Table 3b and the standard deviations in table 7. By taking the biggest mean difference values, all other differences will result in better P-values. Hence, speed 6.4 and 1.6 for the 10 mm sphere had the most prominent gap at 0.53 and 0.51 RCmean respectively.
Plugging both into a t-test calculator [29] along with the correct standard deviations and sample sizes, in this case N = 2 for speed 6.4 and N = 3 for speed 1.6 gives a two tailed P-value of 0.93. By conventional criteria this difference is considered to be not statistically significant. This also means that all other differences would result in P-values superior to the one mentioned earlier thus also being insignificant.
We then applied that same concept using the RC max table 4 this time. We can observe the biggest difference once again between speeds 6.4 and 1.6 this time for the 28 mm sphere with RC max values of 1.18 and 1.10 respectively. The P-value in this case turned out to be 0.73 which once again resulted in an insignificant value statistically with all the others t-test thus having a value superior to 0.73.
Since all the P-values are insignificant for both RCmean and RCmax we can thus pick any of the 3 speeds so long as we use the proper reconstruction parameters and Gaussian filter size. Speed 6.4 would be the quickest of the 3. This could in turn increase patient comfort and throughput since the scans would be performed much faster which is certainly also beneficial.

Whilst the results are very promising and accurate within the given parameters, there were also a few limits to this study.
First and most importantly, is the lack of RCpeak. Using 3D slicer and having to calculate the recovery coefficients manually caused issues solely when faced with the peak values. We thus had to disregard them for this study using only RCmean and max for the accreditation of the Quadra PET/CT scanner.
Secondly, are the issues regarding the smallest sphere at RCmax. Due to increased noise provided by the reasons in section 3.3, the recovery coefficient belonging to the 10 mm sphere did not respect the EARL 2 guidelines. Although the reasons validate the work done, having the chance to repeat and refine the protocol would be ideal.

4 Conclusion

The Quadra PET/CT scanner proved to be a state of the art whole body scanner. This paper unraveled some of its most useful properties, prior to testing its continuous bed motion mode for EARL accreditation. Moreover, the different speeds were tested statistically and were regarded as similar. This allows us to pick the highest speed when using this scanner which will be beneficial towards all parties as it reduces scan time and improves patient comfort and throughput.

In brief, the research questions posed in Section 1.4 are adressed as follows:

A1. When working at continuous bed motion with the correct reconstruction parameters, the effects were noticeable at the 3 speeds relative to the static scan having values above it. This could be due to its weight, injected dose and motion which has been known to reduce image quality, as well as the differences between filter sizes which play a role in noise reduction. However, since the EARL 2 limits were respected, the effects become quite insignificant unless we are diving deep within image quality and other more precise variables. This makes continuous bed motion a great application, that should be used for clinical applications as it will reduce the duration of acquisition significantly.

A2. In this study, we noticed that the ideal reconstruction parameters leading to full compliance would be a whole body image reconstructed with point spread function (PSF) and the time of flight (TOF) module, having a ring difference (MRD) of 85, 4 iterations, 5 subsets, a matrix size of 220 x 220, 708 slices and most importantly a **4 mm Gaussian filter** as the convolution kernel. Furthermore, the reconstructions apply to all speeds since they were deemed similar statistically.

These total body PET/CT scanners have been in development for over a decade bringing progress with the increased sensitivity allowing for faster imaging at lower doses. This in turn can open the door to ultra fast and total body dynamic imaging [30].
When looking to the future, repeating this experiment would thus be necessary as not all accreditation points were complete. The RCmax although coming very close still needs to be slightly adjusted. Furthermore, RCpeak must also be re-performed and properly tested. Although every other aspect of this research does provide some interesting insight on continuous bed motion and its EARL accreditation at varying speeds, using varying reconstruction parameters, these 2 important sections would still be required for a complete study.

Bibliography

[1] D. W. Townsend, "Combined positron emission tomography–computed tomography: The historical perspective," *Seminars in Ultrasound, CT and MRI*, vol. 29, p. 232–235, Aug. 2008.

[2] T. Filleron, "Comparing sensitivity and specificity of medical imaging tests when verification bias is present: The concept of relative diagnostic accuracy," *European Journal of Radiology*, vol. 98, p. 32–35, Jan. 2018.

[3] I. Rausch, J. G. Mannheim, J. Kupferschläger, C. la Fougère, and F. P. Schmidt, "Image quality assessment along the one metre axial field-of-view of the total-body biograph vision quadra pet/ct system for 18f-fdg," *EJNMMI Physics*, vol. 9, p. 87, Dec. 2022.

[4] I. Alberts, J.-N. Hünermund, G. Prenosil, C. Mingels, K. P. Bohn, M. Viscione, H. Sari, B. Vollnberg, K. Shi, A. Afshar-Oromieh, and A. Rominger, "Clinical performance of long axial field of view pet/ct: a head-to-head intra-individual comparison of the biograph vision quadra with the biograph vision pet/ct," *European Journal of Nuclear Medicine and Molecular Imaging*, vol. 48, p. 2395–2404, July 2021.

[5] J. H. University, "Positron emission tomography (pet)," Aug. 2021.

[6] lab admin, "Enhancing pet/ct sensitivity accuracy," Aug. 2023.

[7] S. Surti, A. R. Pantel, and J. S. Karp, "Total body pet: Why, how, what for?," *IEEE Transactions on Radiation and Plasma Medical Sciences*, vol. 4, p. 283–292, May 2020.

[8] E. Calderón, F. P. Schmidt, W. Lan, S. Castaneda-Vega, A. S. Brendlin, N. F. Trautwein, H. Dittmann, C. la Fougère, and L. S. Kiefer, "Image quality and quantitative pet parameters of low-dose [18f]fdg pet in a long axial field-of-view pet/ct scanner," *Diagnostics*, vol. 13, p. 3240, Jan. 2023.

[9] W. Siman and S. C. Kappadath, "Comparison of step-and-shoot and continuous-bed-motion pet modes of acquisition for limited-view organ scans," *Journal of Nuclear Medicine Technology*, vol. 45, p. 290–296, Dec. 2017.

[10] EANM, "History – eanm."

[11] R. Boellaard, R. Delgado-Bolton, W. J. G. Oyen, F. Giammarile, K. Tatsch, W. Eschner, F. J. Verzijlbergen, S. F. Barrington, L. C. Pike, W. A. Weber, S. Stroobants, D. Delbeke, K. J. Donohoe, S. Holbrook, M. M. Graham, G. Testanera, O. S. Hoekstra, J. Zijlstra, E. Visser, C. J. Hoekstra, J. Pruim, A. Willemsen, B. Arends, J. Kotzerke, A. Bockisch, T. Beyer, A. Chiti, and B. J. Krause, "Fdg pet/ct: Eanm procedure guidelines for tumour imaging: version 2.0," *European Journal of Nuclear Medicine and Molecular Imaging*, vol. 42, no. 2, p. 328–354, 2015.

[12] A. Kaalep, C. N. Burggraaff, S. Pieplenbosch, E. E. Verwer, T. Sera, J. Zijlstra, O. S. Hoekstra, D. E. Oprea-Lager, and R. Boellaard, "Quantitative implications of the updated earl 2019 pet–ct performance standards," *EJNMMI Physics*, vol. 6, p. 28, Dec. 2019.

[13] EANM, "Accreditation specifications – eanm earl – research4life."

[14] S. Healthineers, "Biograph vision quadra pet/ct scanner - siemens healthineers."

[15] G. A. Prenosil, H. Sari, M. Fürstner, A. Afshar-Oromieh, K. Shi, A. Rominger, and M. Hentschel, "Performance characteristics of the biograph vision quadra pet/ct system with a long axial field of view using the nema nu 2-2018 standard," *Journal of Nuclear Medicine*, vol. 63, p. 476–484, Mar. 2022.

[16] Gammadata, "Nema iec pet body phantom."

[17] D. Koopman, J. A. C. van Osch, P. L. Jager, C. J. A. Tenbergen, S. Knollema, C. H. Slump, and J. A. van Dalen, "Technical note: how to determine the fdg activity for tumour pet imaging that satisfies european guidelines," *EJNMMI Physics*, vol. 3, p. 22, Sept. 2016.

[18] J. V. Sluis, P. v. Snick, A. Brouwers, W. Noordzij, R. Dierckx, R. Borra, A. Lammertsma, A. Glaudemans, C. Tsoumpas, and R. Boellaard, "Earl compliance of the biograph vision quadra pet/ct," *Journal of Nuclear Medicine*, vol. 63, p. 3307–3307, Aug. 2022.

[19] M. A. Ashraf and A. Goyal, *Fludeoxyglucose (18F)*. Treasure Island (FL): StatPearls Publishing, 2024.

[20] P. M. O. Gomes, A. M. S. Silva, and V. L. M. Silva, "Pyrazoles as key scaffolds for the development of fluorine-18-labeled radiotracers for positron emission tomography (pet)," *Molecules*, vol. 25, p. 1722, Jan. 2020.

[21] H. I. Academy, "Point spread function (psf)."

[22] G. Akamatsu, K. Ishikawa, K. Mitsumoto, T. Taniguchi, N. Ohya, S. Baba, K. Abe, and M. Sasaki, "Improvement in pet/ct image quality with a combination of point-spread function and time-of-flight in relation to reconstruction parameters," *Journal of Nuclear Medicine*, vol. 53, p. 1716–1722, Nov. 2012.

[23] F. P. Schmidt, J. G. Mannheim, P. M. Linder, P. Will, L. S. Kiefer, M. Conti, C. la Fougère, and I. Rausch, "Impact of the maximum ring difference on image quality and noise characteristics of a total-body pet/ct scanner," *Zeitschrift Fur Medizinische Physik*, pp. S0939–3889(23)00113–7, Oct. 2023.

[24] D. slicer, "3d slicer image computing platform."

[25] *Chapter 11 - Oncology: Positron Emission Tomography*, p. 227–264. Philadelphia: W.B. Saunders, Jan. 2014.

[26] A. K. Pandey, P. Sharma, M. Pandey, K. Aswathi, A. Malhotra, and R. Kumar, "Spreadsheet program for estimating recovery coefficient to get partial volume corrected standardized uptake value in clinical positron emission tomography-computed tomography studies," *Indian Journal of Nuclear Medicine: IJNM: The Official Journal of the Society of Nuclear Medicine, India*, vol. 27, no. 2, p. 89–94, 2012.

[27] I. Eng., "Image noise - image engineering."

[28] Y. Tsutsui, S. Awamoto, K. Himuro, Y. Umezu, S. Baba, and M. Sasaki, "Edge artifacts in point spread function-based pet reconstruction in relation to object size and reconstruction parameters," *Asia Oceania Journal of Nuclear Medicine and Biology*, vol. 5, no. 2, p. 134–143, 2017.

[29] Graphpad, "T test calculator."

[30] Y. Sun, Z. Cheng, J. Qiu, and W. Lu, "Performance and application of the total-body pet/ct scanner: a literature review," *EJNMMI Research*, vol. 14, p. 38, Apr. 2024.

[31] P. Bhandari, "Normal distribution — examples, formulas, uses," Oct. 2020.

[32] A. M. Winkler, "Gaussian kernels: convert fwhm to sigma," Aug. 2011.

Appendices

A Sigma to FWHM conversions

Smoothing of images and functions uses Gaussian Kernels. Often, conversions are required to go from the full width half maximum value to the standard deviation of the filter sigma (σ). This is required since most image analysis programs will have the implementations based on the sigma values.
The probability density function for the Gaussian distribution is applied to determine the FWHM values.

$$f(x) = \frac{1}{\sigma\sqrt{2\pi}} \exp^{-\frac{(x-\mu)^2}{2\sigma^2}} \tag{3}$$

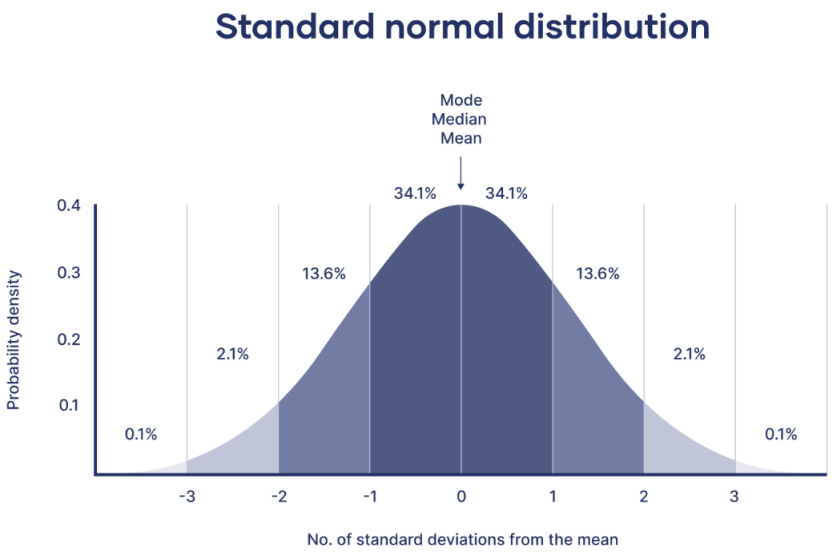

[31]

So, if the filter is centered at the origin this would mean that the mean is 0 and the FWHM would be the distance between $-x_s$ and $+x_s$ which in turn produce half the peak.
This being said, x_s should be calculated.

$$f(x_s) = f(\mu)/2 \tag{4}$$

$$\frac{1}{\sigma\sqrt{2\pi}} \exp^{-\frac{(x_s)^2}{2\sigma^2}} = \frac{1}{2}\frac{1}{\sigma\sqrt{2\pi}} \tag{5}$$

For situations where σ is $\neq$ to 0, we can solve for x_s.
This gives:

$$x_s = \pm\sqrt{2\sigma^2 ln2} \tag{6}$$

Now that x_s has been obtained, FWHM is simply $2x_s$
This finally gives us:

$$FWHM = 2\sqrt{2\sigma^2 ln2} = \sigma\sqrt{8ln2} \tag{7}$$

Since $\sqrt{8ln2} = 2.355$, then FWHM = $\sigma * 2.355$ [32]

These calculations to facilitate conversions will be beneficial when modifying our originally provided images by filtering in order to obtain more accurate results as seen in section 2.5 which describes shortly how the filtering feature using this sigma value was applied.